BARC

NEWSLETTER

भाभा परमाणु अनुसंधान केंद्र
BHABHA ATOMIC RESEARCH CENTRE

IN THIS ISSUE

C O N T E N T S

INDIGENOUS SWITCH-ROUTERS FOR DEPENDABLE VIDEO SURVEILLANCE NETWORKS

Electronics and Instrumentation Group

Video-surveillance represents a security sensitive application and usually consists of number of geographically distributed cameras (fixed and PTZ type) connected to a farm of high performance servers (for display, recording, storage) through computer network. Currently all network devices are of foreign origin leading to cyber security concerns in critical applications. Now, we have an indigenous solution for dependable and secure surveillance network.

Carrier Ethernet based switch-routers designed by IIT-Bombay are being manufactured under license by ECILas ECR series products. E&I group of BARC is involved in adding value to this path-breaking new technology through enhancements and evaluation studies so as to increase its penetration in security sensitive and strategic applications. ECR routers with their proprietary routing protocols are well-suited for closed group communication where cyber-security is a concern. This, along with low latency and low power make them especially attractive option for integrating video-surveillance networks spanning 10's of Kms and thousands of cameras.

Currently,three models (Fig.1: ECR-100/1000/1010) are available. Together, they provide both copper and optical Ethernet ports and support 10/100/1000 Mbps speeds as well as 10Gbps Ethernet or OTN. A light-weight Network Management System(NMS)

helps in configuration, operation, monitoring and maintenance of the network. The network is "completely managed"- all communication parameters are a-priori configured from NMS. Only the configured nodes are allowed to communicate with other configured nodes and the traffic is limited to the provisioned bandwidth. This feature greatly enhances security sinceaccessto network is restricted to configured, authorized users/ devices.

Salient features of ECR based networks are given below.
➢ Provides a high level of protection against DoS (Denial of Service) attacks.
➢ Inherent topology security provides data-origin authentication.
➢ Configuration change and download is authorized and authenticated before being accepted and is maintained on power-on/off.
➢ Replay of control plane traffic for configuration is protected through timeout of authentication and session tokens
➢ Any fault in the network is detected and switchover to pre-defined redundant path occurs within 50msec and is annunciated on NMS.

E&I group of BARC has successfully integrated a prototype Video Surveillancesystem around these ECR switch-routers.Specific functions were added to the

Fig.1: ECR100, ECR1000 and ECR1010
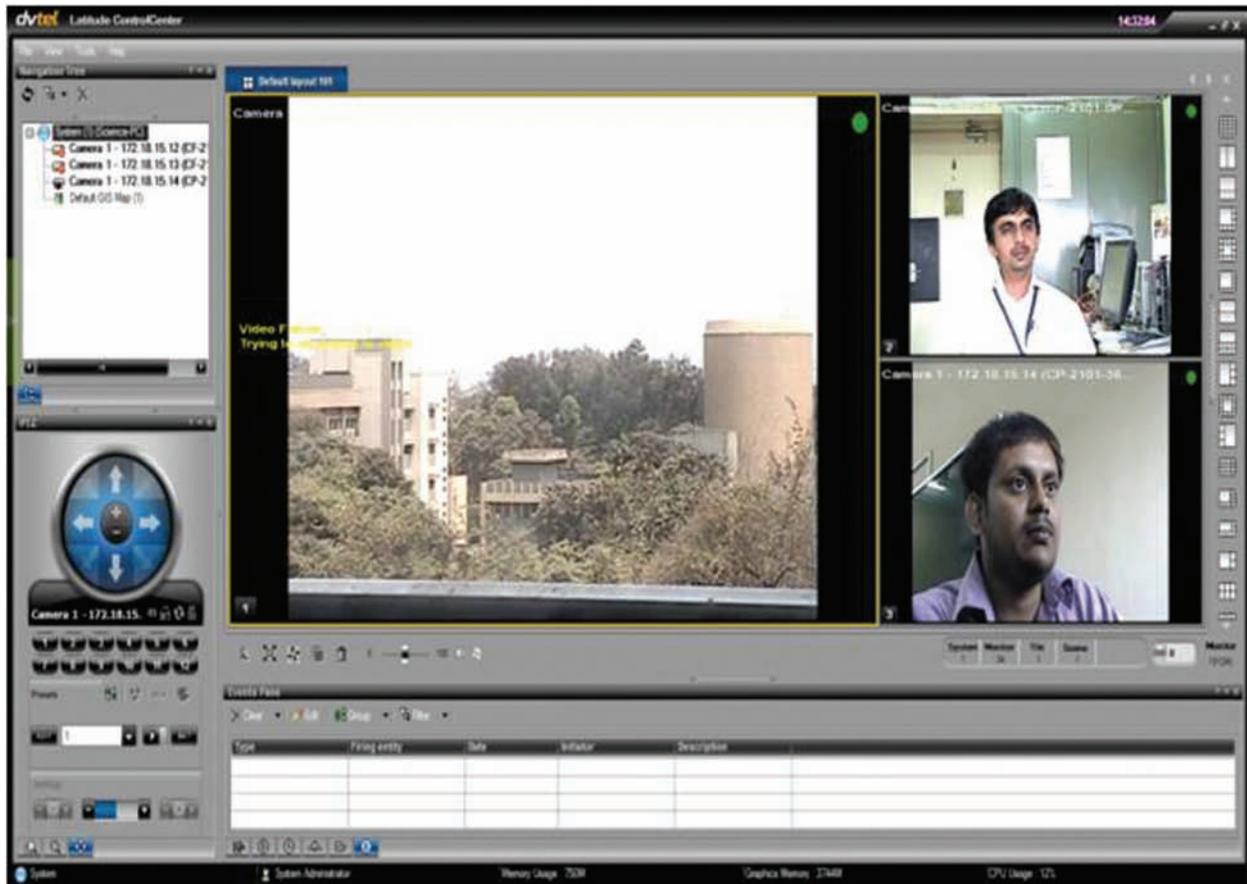
Fig.2: VMS screenshot of 3 cameras

devices to optimize their performance in a video- surveillance application. These include Internet Group Management Protocol (IGMP)for dynamic join and leave for multicast group and provision to handle burst of traffic from cameras without incurring delays and freeze-frames.Fig.2 shows the screenshot of display workstation fornetwork with 3 cameras.

ECR routers are well-suited for demanding video-surveillance applications; itoffers an indigenous, dependable, secure and economical alternative for security sensitive installations while planning their video-surveillance systems.

New Approach for Control Rod Position Indication System for Light Water Power Reactor

Sushil Bahuguna, Sangeeta Dhage, Nawaj S., Salek C., S.K. Lahiri and P. P. Marathe

Control Instrumentation Division

and

S. Mukhopadhyay

Seismology Division

and

Y.K. Taly

BARC Safety Council

Abstract :

Control rod position indication system is an important system in a nuclear power plant to monitor and display control rod position in all regimes of reactor operation. A new approach to design a control rod position indication system for sensing absolute position of control rod in Light Water Power Reactor has been undertaken. The proposed system employs an inductive type, hybrid measurement strategy providing both analog position as well as digital zone indication with built-in temperature compensation. The new design approach meets single failure criterion through redundancy in design without sacrificing measurement resolution. It also provides diversity in measurement technique by indirect position sensing based on analysis of drive coil current signature. Prototype development and qualification at room temperature of the control rod position indication system (CRPIS) has been demonstrated. The article presents the design philosophy of control rod position indication system, the new measurement strategy for sensing absolute position of control rod, position estimation algorithm for both direct and indirect sensing and a brief account associated processing electronics.

Introduction

Reactor power is controlled by maneuvering solid absorber rods (called control rods) inside a reactor core. True position of the control rod, measured from the bottom of the core is required to be known for reliable and safe operation of the reactor. Motion of the control rod is imparted by Control cum Shutoff Rod Drive Mechanism (CSRDM). Latch type magnetic jack mechanisms are used in most of the Light Water Reactors (LWRs) across the world, as these mechanisms are inherently fail-safe. Moreover as there is minimal on-load relative movement between the moving parts, the wear is negligible which in turn guarantees long service life. Fig. 1 shows the sectional view of a typical CSRDM. Out of core (top and bottom limit), zone and intermediate rod position information are needed for plant control as well as for status-feed to
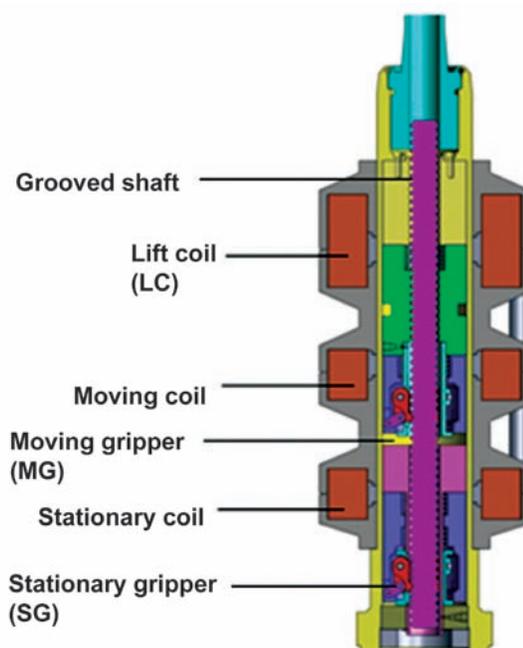
Fig. 1: Sectional View of CSRDM

the operator. In Light Water Power Reactors the rod is moved typically in steps of 10-20 mm and total travel is about 3500-4000 mm.

The kinematic parts of the control rods and the drive mechanism in a Light Water Power Reactor are in contact with high temperature PHT water. PHT water temperature varies from 30°C to 330°C (from reactor start up to full operational mode). Different linear sensing technologies were studied to home in on a rugged and reliable design for the position sensing of the control rods that would work for this wide range of temperature. Commonly used permanent magnet and reed type position sensors do not work reliably at high operating temperature. Similarly, high temperature and radiation rule out the use of semiconductor sensors. Moreover, both reed type and semiconductor sensors are generally used as switches. As a consequence, measurement resolution with these sensors becomes limited by the number of sensors used and their physical dimension [1].

An inductive type linear position sensor is primarily preferred for CRPIS due to its simplicity of construction, low cost and ruggedness. Wide variation of temperature however, causes substantial variation in resistance of the sensor coil. This variation in resistance is compensated by winding the coil with the wire having very low value of temperature coefficient of resistance, so that the change in the inductive sensor output with temperature is negligible. The problem can also be circumvented by designing a special circuit which would measure the inductance and resistance independently but simultaneously. Measured resistance variation due to temperature can be used to provide a compensation for the temperature dependent component of the signal in the output of the sensor coil. A reference coil is generally used for compensation whose inductance is zero (Null coil) and resistance is same as that of the sensor coil.

Inductive type sensors are in common use for control rod position monitoring in nuclear power plants (NPP). In [2] rod position measurement detector is made up of a primary coil and a secondary coil covering the

entire height of the grooved shaft guide housing. The magnetic coupling between the primary and secondary coil depends on how far the rod drive shaft is inserted into the tubular coils. It provides analog measurement of the position of the rod. The design in [3] also uses similar kind of analog rod position measurement detector comprising of a primary and a secondary coil. The limitation of these designs is that the rod drive shaft (grooved shaft) needs to be magnetic over its full travel length.

Newer designs of position indication system have subsequently employed digital measurements and inductive type sensors are used as digital switches. In [4] inductive type position sensing system is a digital measurement system. The position sensor works on the principle of a low frequency transformer. This transformer has one primary and several secondary coils. The core is made up of a sequence of magnetic (magnetic shunt) and non magnetic parts. Due to the magnetic core features, induced voltage on secondary transformer coils is changed in accordance with magnetic or non magnetic part of the core. Combination of voltage level on secondary coil windings gives the binary code of control rod position with an accuracy of ±1 step (20 mm)

A systematic approach was adopted for the indigenous development of CRPIS with the objective to reliably measure the absolute position of the control rod. A new design of linear inductive sensor has been proposed based on the results of the proof of concept experiments and the study on existing technologies. The design precludes the need for temperature compensation by designing the inductive sensor with three (primary, secondary and tertiary) coils where primary is energized by a constant current source. Secondary outputs are measured to give position within zone and the tertiary coil output gives zone information (explained later). Variation of temperature does not affect the secondary output as exciting magneto motive force remains constant due to constant current primary excitation. A prototype system was developed and demonstrated for full 4000mm travel of the control rod.

Overview of the proposed CRPIS design

A new hybrid measurement (analog and digital) approach of design methodology has been adopted for the development of the prototype CRPIS. It provides ruggedness, reliability and redundancy in measurement while retaining simplicity in the design. In the proposed design sensor assembly is put outside the pressure boundary of CSRDM and the grooved shaft is also non magnetic. The CRPIS system has two diverse methods of measurement A) Inductive sensor based absolute rod position measurement and B) Indirect position measurement based on the current signature of CSRDM drive coil. Fig. 2 shows the overall system block diagram. The system is composed of a rod position sensor coils mounted on grooved shaft guide housing, electronics for conditioning and processing of the signal from sensor coils and drive coils to indicate both the absolute rod position and step movement count. The total coil stack housing of 4000mm length is divided in 10 zones each of 0.4 meter length. In each individual zone, 4 coils (each having three windings, primary, secondary and tertiary) are stacked vertically. Each of these coils is approximately 100 mm long. The tertiary windings of all the four coils in a particular zone are connected in
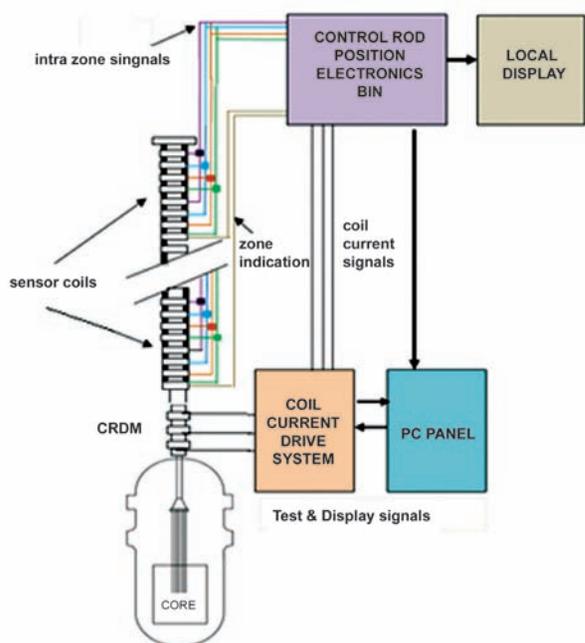
Fig. 2: System Block Diagram

series to monitor zonal position of the rod. The tertiary circuit acts as a switch and provides information indicating if the rod is present in that zone. The digital information is latched by the electronics. In the triple-wound coil, primary coil is energized by a constant current source and the induced voltage in secondary and tertiary coils are measured to find the continuously changing position of the control rod. The system can be considered hybrid, providing both analog position (by secondary) as well as digital zone indication (by tertiary).The primary, secondary and tertiary coil windings are isolated by providing proper insulation layers between them. The overall scheme provides galvanic isolation between excitation and measurement circuits.

A) Inductive sensor based absolute rod position measurement

The proposed inductive sensor based absolute rod position measurement scheme has the merit of inbuilt temperature compensation for the variation in temperature in the reactor core. The actuator, also called magnetic slug is a 100mm long piece, made up of ferromagnetic stainless steel AISI grade SS430 and is attached to the top of the control rod. Due to movement of the control rod, the gripper rod moves in turn moving the magnetic slug. In the presence of magnetic core material, flux linkage increases between the primary and secondary/ tertiary coils which causes consequent increase in the secondary/ tertiary output voltages. The description of the scheme, corresponding sensor arrangements and the working principle, are explained in the following sub sections.

Sensor coil unit and power supply

The arrangement of windings in sensor coil unit is shown in Fig. 3. The sensor coil in the prototype system is made of copper enameled wire and is designed to work at 200ºC. The acceptable manufacturing tolerance in sensor parameters is $\pm$ 3% of the desired value to maintain the measurement accuracy. For higher operating temperature (300 ºC) the sensor coil could be made of Nickel clad Copper (ceramic
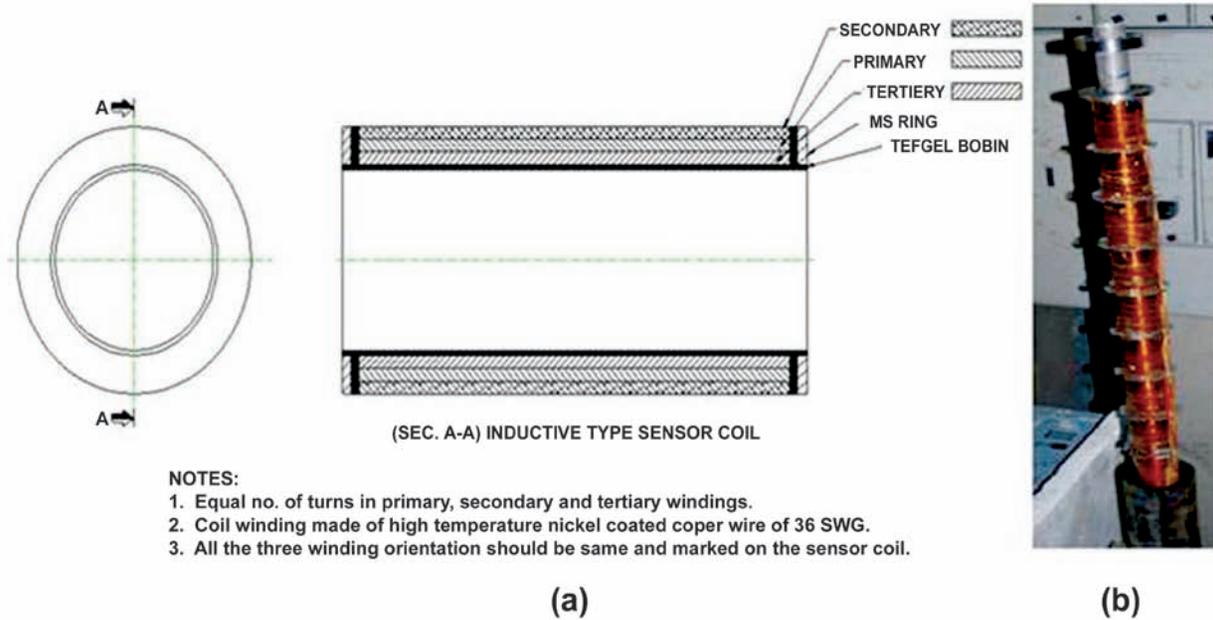
Fig.3: (a) A sensor coil unit (b) 40 number of such sensors assemblies

Table 1: Sensor coil input and output

Sensor Coil primary circuit input		Sensor Coil Secondary circuit output	
Peak to Peak Current	14 m Amp	Output voltage without slug	$80\,V_{PP}$
Frequency	50 Hz	Output voltage with slug	$102\,V_{PP}$
Voltage	200 V	Output variation obtained due to presence of slug	$22\,V_{PP}$

insulated) or mineral insulated wire. Four constant current sources are needed to excite four primary circuits. Primary and secondary coil circuit input and output are shown in Table 1.

Working Principle

The position indication sensor works on the principle of electromagnetic induction. Magnetic flux produced by the primary coil current links with both the secondary and tertiary coils and induces electromotive force (EMF) in both. In the presence of the magnetic slug, flux linkage is larger compared to when it is absent. The change in the flux linkage causes the change in coil inductance and also in the induced voltages in the secondary and tertiary. This change in voltage is used for detection of the actuator. The voltage (EMF) induced in the secondary due to linkage of flux from the primary is given by

$$V = -\mu\left(\frac{N^2 A}{L}\right)\frac{dI}{dt} \qquad (1)$$

where, N = Number of the turns in the coil, I = Current in the coil in Amp, μ = Permeability inside the coil, A = Area of the coil in m2 and L = Length of the coil in meter.

Once the coil design and primary excitation are fixed all the parameters in the above equation are constant except the permeability (μ) of the core. In the presence of magnetic slug inside the coil the permeability increases and hence the voltages induced in the secondary and tertiary coils increase. However, as the magnetic slug enters and leaves a coil the extent of magnetic coupling changes giving rise to non-linearity in the measurement.

Detection Scheme

In order to reduce the number of wires and to increase redundancy, coils are connected in a particular sequence. To understand the configuration clearly, let us index coils in a zone as 1, 2, 3 and 4. Coils with the same index in all the 10 zones are connected in series to form one circuit. So there are 4 primary and 4 secondary circuits. All four tertiary winding in a particular zone are connected in series as mentioned earlier. Thus there are ten tertiary circuits. The outputs of all the 14 (4 secondary plus 10 tertiary) measurement circuits are acquired after signal conditioning and are further processed in a DSP based system. Sensor coil interconnections only for two zones (Z1 and Z2) with four secondary measurement circuits (S1, S2, S3 and S4) are shown in Fig.4.
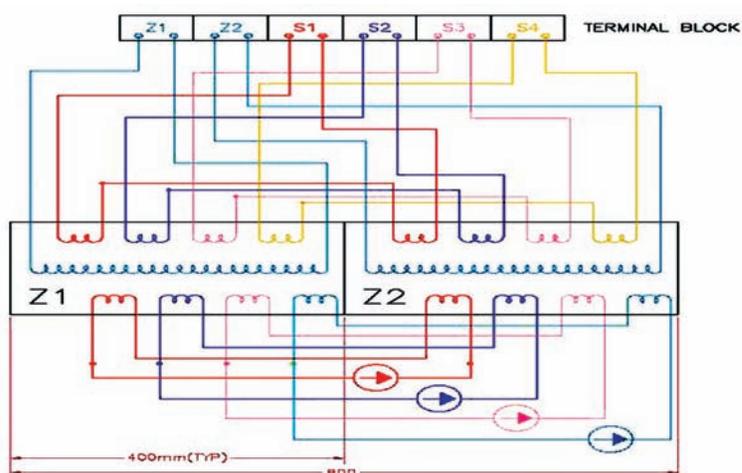
Fig.4: Sensor coil interconnection only for two zones

Each of the four primary circuits is excited by separate current source to avoid common mode failure. This scheme also provides a good measure of redundancy in case of failure of single coil (circuit). When the residence circuit (where magnetic slug is present) fails, the neighboring coils provide the necessary position information without sacrificing the measurement resolution. Information related to the faulty circuit is displayed on the LCD/PC besides the position information.

A DSP based signal processing unit acquires data of four secondary and ten tertiary circuits' output. The processing algorithm computes RMS voltage for each output. RMS outputs of tertiary are compared with zone threshold for zone detection. To find the position of the rod within the zone, two threshold levels are selected for the comparator with hysteresis. Thresholds are decided based on the design requirement, environmental conditions and change in output voltage with and without magnetic actuator (22V peak to peak). Position resolution of 50 mm has been achieved with two levels of thresholding. Higher resolution may be achieved with the increase in the number of threshold levels. The algorithm calculates the position based on the following formula.

$$D = 400(Z-1) + 100(S-1) + 50T \qquad (2)$$

where 'D' is absolute position of control rod in mm. 'Z' is zone number where control rod/ magnetic slug is detected ($1 \leq Z \leq 10$). 'S' is the number for the secondary coil circuit where control rod is detected ($1 \leq S \leq 4$). Similarly T is threshold number crossed by secondary output ($0 \leq T \leq 2$).

The output from the two neighboring secondary coil circuits with two threshold levels (T1 & T2) is shown in Fig. 5. The curve shows that redundant position information can be found for same location of the slug as it moves out of one sensor coil and enters the next. In case one coil circuit fails, measurement resolution still remains the same (50 mm) as it is possible to detect rod position from the output of the two neighboring
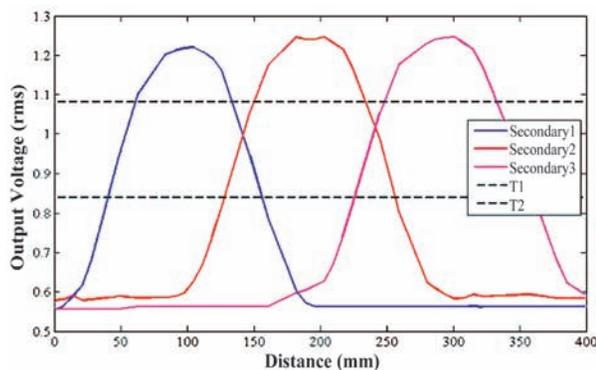
Fig.5: Sensor coils output with movement of slug

coils. Single sensor coil failure algorithm computes the position based on the following formula.

$$D = 400(Z-1) + 100S + 50(2-T) \qquad (3)$$

B) Indirect position measurement based on current signature of CSRDM drive coils

In a CSRDM three electromagnetic coils namely stationary gripper (SG), moving gripper (MG) and lifting coil (LC) are mounted outside the pressure boundary as shown in Fig 1. Stationary gripper holds or releases the drive rod and supports the load of the drive assembly. Movable gripper holds the drive rod when it moves. Lifting coil lifts the drive rod held by the movable gripper. These coils and armatures are energized in a pre-programmed manner to raise and lower the drive rod. Coils are energized based on the commands from control rod drive system (CRDS). However, position feedback is not available for the step movement. The indirect position measurement is a technique for sensing step movement based on

current signals analysis of SG, MG and LC coils of CSRDM [5]. The coil currents have transients (notch) as shown in Fig.6 due to butting of the armature signifying physical movement of the control rod. These notches indicate that the drive rod has actually moved by a step.
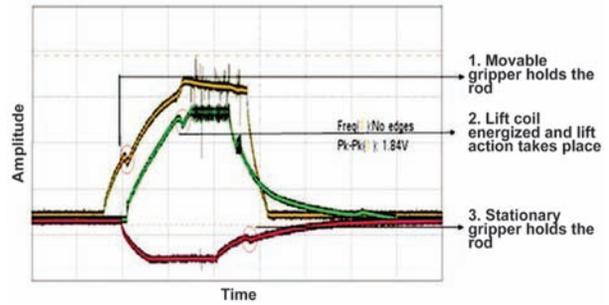
Fig.6: Current coil signals of MG, LC and SG coils

Current signals are acquired continuously by the data acquisition system of CRPIS. The direction of movement is detected by analyzing the sequence of excitation of the three coils. During the mechanical latching operation of gripper, a notch is observed in the current waveform of the gripper coil. The notch
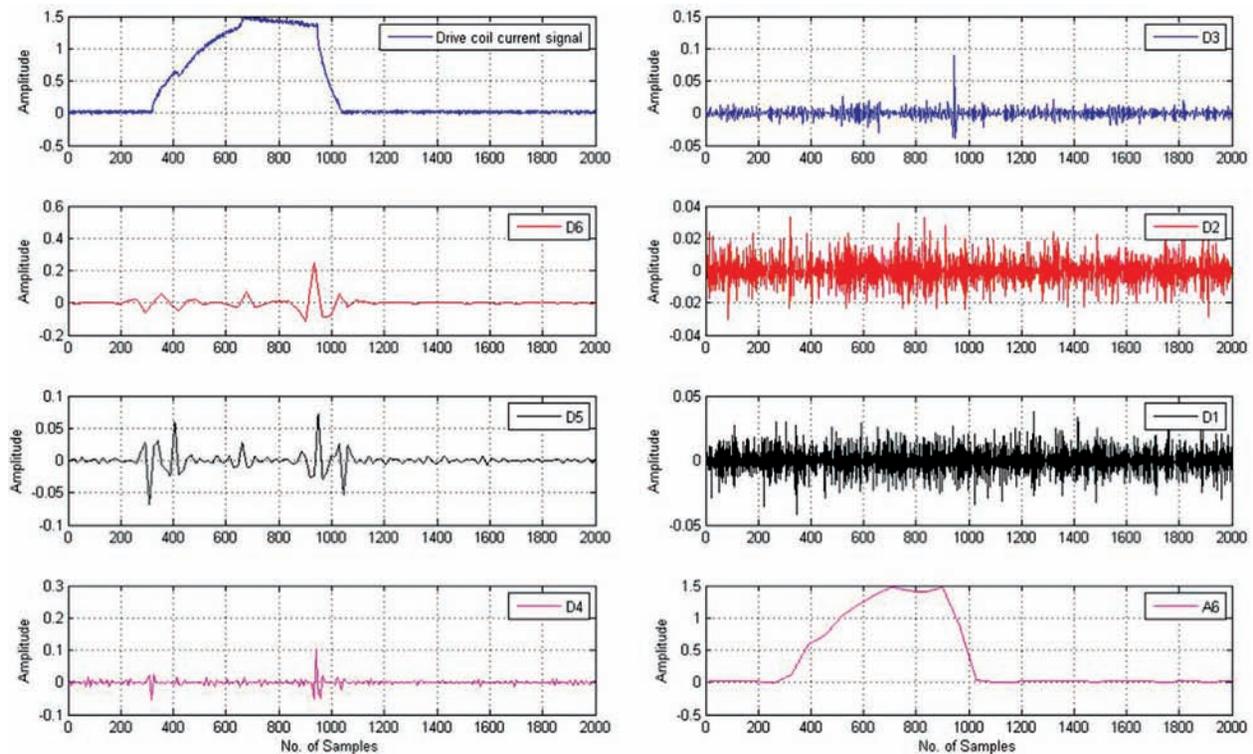
Fig. 7: Drive coil current signal and its Wavelet Decomposition in six frequency bands (D1 - D6 and A6)

is detected by running a wavelet based detection algorithm. Discontinuities in the coil current signature and the notch corresponding to drive rod movement have different frequency characteristics. These two patterns can be distinguished by their appearance in different frequency bands in wavelet decomposition. The current signals of all the three coils are decomposed into six different frequency bands (scales) by using discrete Biorthogonal filter banks. The drive coil current signal, six levels decomposition (D1-D6) and approximation (A6) at the coarsest scale are shown in Fig.7. The notch due to control rod movement appears in 5th detail coefficient (D5) scale whereas other discontinuities due to coil current excitation pattern are present in other detail coefficients too. By finding maxima-minima on D5 and with suitable thresholding, the notch is identified. Summation of D4 (4th detail coefficient) and D5 coefficients could also be used to identify notch in some cases where D5 alone is not sufficient, as shown in Fig.8. The step movement is assured by observing the correct sequence of occurrence of notches and time spacing between switching operations. The flow chart for wavelet based notch detection algorithm is shown

in Fig.9. Current profile data is processed in real time and step counter is updated and displayed on Graphical LCD. Wavelet analysis may further be useful to detect aging of the mechanism parts.
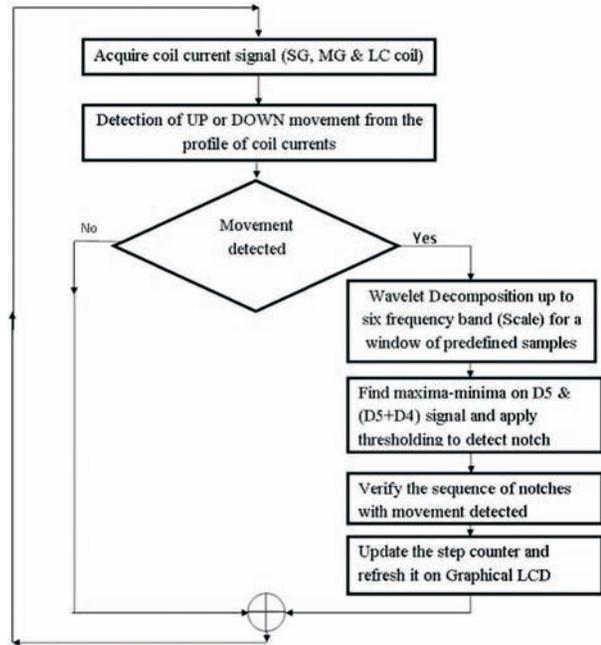
Fig.9: Wavelet based notch detection algorithm for drive coil current signal
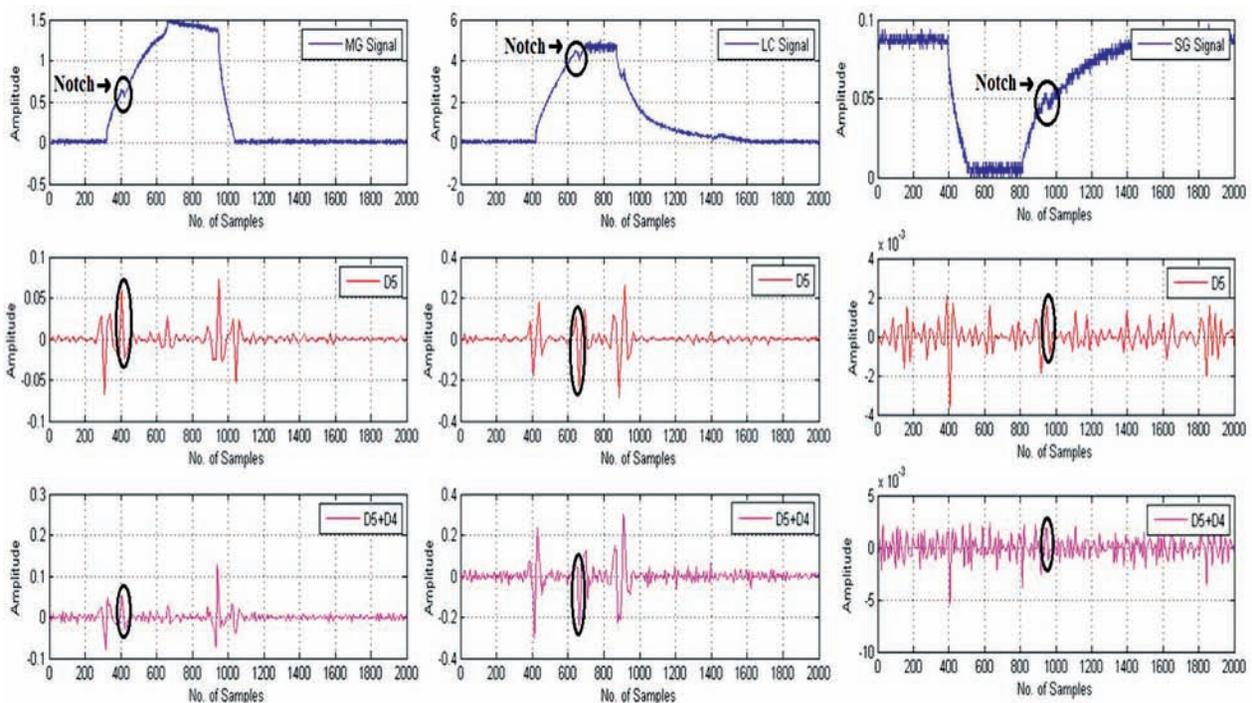
Fig. 8: MG, LC and SG current signal and their D5 and D4+D5 decomposed signal with the detected notch

Detection electronics of CRPIS

There are certain specific merits to replace traditional analog instrumentation and control (I&C) systems in nuclear plants with digital I&C systems, i.e. systems based on computers and microprocessors [6]. The advantages of using FPGA in NPP are discussed in [7]. In some of the advanced Rod Position Instrumentation (RPI), computer units are dedicated to the acquisition and digital processing of the analog rod position measurements. In the present work, both direct and indirect position measurement schemes have been implemented in DSP-FPGA based hardware enabling signal processing in real time. The system consists of five modules i.e. power supply module, constant current source module, signal conditioning module, data acquisition & processing module and output module. The basic block diagram of electronics is shown in Fig. 10. Redundancy in electronics is achieved by using two data acquisition & processing modules in hot standby. Both the units compute the position of control rod independently and display the position on LCD display. The Ethernet port is provided to communicate the control rod position information to control room. CRPIS system is designed for higher availability by increasing testability and maintainability. This is achieved by adding self monitoring feature in
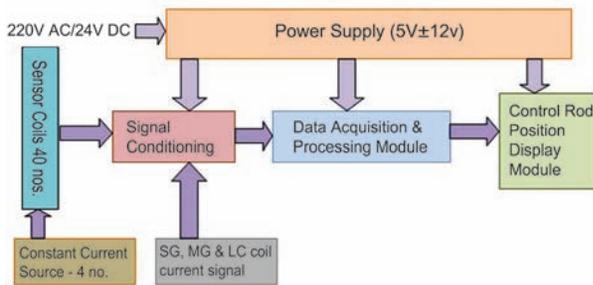
the system and adopting modular design with rack mountable electronics. Technical specification of developed CRPIS system is given in Table 2.

Functional Tests of CRPIS at room temperature

The proof of concept experiment was successfully concluded first for one meter travel (test setup shown in Fig. 11). The functional testing of full scale rod position systems for 4000mm travel was taken up next by augmenting an existing test mechanism. As the grooved shaft moves, the attached magnetic actuator also moves over the inductive sensor coil. Voltage changes on secondary and tertiary coils were sensed and processed in position sensing electronics housed in the interface panel. In order to test the resolution of position sensor command for fixed number of step movement is given from the test consol panel and corresponding movement in mm is checked. This testing is repeated in steps of 50 mm for full travel of 4000mm. Functional testing of sensing system based on wavelet analysis of drive coils' current signature is also conducted. The increment/decrement by 1 step is checked for every step movement of 10mm. During the functional test, position of the control rod in different zones and inside a zone is displayed. Healthiness of 14 measurement circuits is also displayed on the LCD/PC panel. System redundancy test is performed in a zone by simulating "single secondary/tertiary circuit failure" condition. It is observed that measurement resolution remains same (50 mm) as that in healthy condition even when a coil circuit fails. System diversity and repeatability tests have also been performed as per the test plan and the prototype system cleared the tests successfully.

Fig.10: Block diagram of CRPIS hardware

Table 2: Technical Specification for control rod position indication system

Sr. No.	Parameter	Value
1	Full Scale Range(FSR) available (Range)	0-4000mm
2	Position Resolution	50mm
3	Position Accuracy	± 30mm
4	Measurement Time	20 m sec
6	Sensor Design temperature	0 - 200° C
7	Working ambient temperature for electronics	-40 - 55° C
8	Power supply	100V DC

Fig. 11: Test setup for proof of concept for 1 meter and 4 meter travel

Conclusion

A prototype position indication system for the control rods of Light Water Power Reactor has been developed. The design employs an inductive type, hybrid measurement system with built-in temperature compensation providing both analog position as well as digital zone indication. Redundancy in the sensing system is provided by specific arrangement of sensor coils and switching to a new position sensing algorithm on detection of a failure without deploying additional set of sensors. Separate excitations for all four primary circuits and hot standby processing electronics further provide redundancy in the detection electronics. Measurement resolution of 50 mm is achieved that remains unchanged in case of failure of one measurement coil circuit. It also provides diversity in measurement technique by using indirect position measurement of drive coil current signature. Prototype development and room temperature qualification of CRPIS has been demonstrated. Experimental evaluation of system performance in the presence of external magnetic field and at higher operating temperature will be taken up in next phase of the project. Wavelet based analysis of drive coils' current signature, to detect aging of the mechanism's moving parts, is also under future scope of work.

References

1. Joseph E. Kowles, David A. "Nuclear control rod position indication system", U.S. Patent Application Publication, Pub. No.: US 2012/0155596 A1, Jun. 21, 2012, https://www.google.co.in/patents/US20120155596 (accessed June 2013)

2. UK-EPR Fundamental Safety Overview, Volume-2: Design and Safety, Chapter-C: Design Bases and General Layout, Section 4.2.4. Position Indicators. http://www.epr-reactor.co.uk/ssmod/liblocal/docs/V3/Volume - Design and Safety/2.C – Design Basis and General Layout/2.C.6.4 - Control-Rod Drive Mechanism - v2.pdf (accessed October 2013).

3. Westinghouse Technology System Manual, Section-8.2, Rod Position Indication (Analog), pbadupws.nrc.gov/docs/ML1122/ML11223A253.pdf (accessed October 2013)

4. Jan Jaňour, "The "Sandra Z100" in position evaluation system for control rods in VVER 1000",Conference VVER 2013, 11-13November 2013, Prague, Czech Republic.

5. Kim et al., "Method for recognizing step movement sequence of control rod drive mechanism of nuclear reactor", U.S. Patent. No.: US 7505545 B2, March 17, 2009, http://www.google.co.in/patents/US7505545. (accessed April 2013)

6. "Instrumentation and Control (I&C) Systems in Nuclear Power Plants: A Time of Transition",https://www.iaea.org/About/Policy/GC/GC52/GC52InfDocuments/English/gc52inf-3-att5_en.pdf (accessed Jan, 2014).

7. Anton Andrashov, "Implementation of Digital Instrumentation and Control Systems (I&C) for Nuclear Power Plants (NPPs) using FPGA-technology: Benefits and Solutions", LAS-ANS 2013, June 24–28, 2013, Buenos Aires, Argentina.

Design & Development of 3D Stereoscopic Visualization System for Surgical Microscope

Pritam Prakash Shete, Dinesh Sarode and Surojit Kumar Bose
Computer Division

Abstract :

Human brain is the most vital organ, which makes neurosurgery as one of the most challenging surgery. Doctors and practitioners undergo extensive neurosurgery training, before they can operate on live human being. The 3D stereoscopic visualization system is more effective during such training. In this article, we discuss design and development of such system for surgical microscope. We describe system architecture, implementation details and overall system competency. The developed system is deployed at Neurosurgery Skills Training Facility, Department of Neurosurgery, AIIMS, New Delhi and is being explored as low cost alternative to commercial systems for conducting neurosurgery skills training sessions.

Introduction

Human brain is the most vital organ, which makes neurosurgery as one of the most challenging surgery. Neurosurgeons undergo extensive neurosurgery skills training and education, before they can operate on live human being. The surgical microscope does provide a stereoscopic view to the surgeon performing the surgery through the eyepieces, but it is ergonomically stressful. Also, the assistants or new practitioners watching the live surgery on the display only get a two-dimensional view captured from the microscope. The comfortable three-dimensional stereoscopic view of the surgical field has become an absolute necessity.

Recently Computer Division, BARC has designed and developed a stereoscopic visualization system for surgical microscope [1] for Neurosurgery Education and Training School (NETS), Department of Neurosurgery, AIIMS, New Delhi. They are engaged in conducting skills training sessions, programs and workshops to provide detailed hands-on skills training to educate MCh, DNB and MD as well as certified neurosurgery professionals from India and other countries. The stereoscopic systems are functionally very close to our human vision system and depth information further improve the experience of new practitioners as the familiar anatomical structures are clearly depicted while undergoing training. NETS is keen to use it to improve the clinical training

productivity. They proposed to develop it from ground up as the commercial systems available are costly and not flexible enough to customize and extend further as per the scenarios.

In this article, we discuss system architecture and challenges faced while developing the real-time stereoscopic vision system for neurosurgery training. See [1] and [2] for more implementation details.

System Architecture

In this section, we discuss system architecture of in-house developed stereoscopic vision system called as the Trimiti system. It consists of hardware components such as stereo acquisition unit, workstation for stereo image processing, 3D display devices and in-hose developed software.

A. Stereo acquisition unit

The surgical microscope uses two separate optical paths with two objectives and two eyepieces to provide slightly different view to the left and right eyes thus providing the stereoscopic view of the field. The addition of the beam splitter in the two optical paths of the microscope provides the way to acquire the left and right images without disturbing the view through the eyepieces. Thus the stereo acquisition unit is realized by using the dual port beam splitter and attaching the two IP cameras to the ports of the
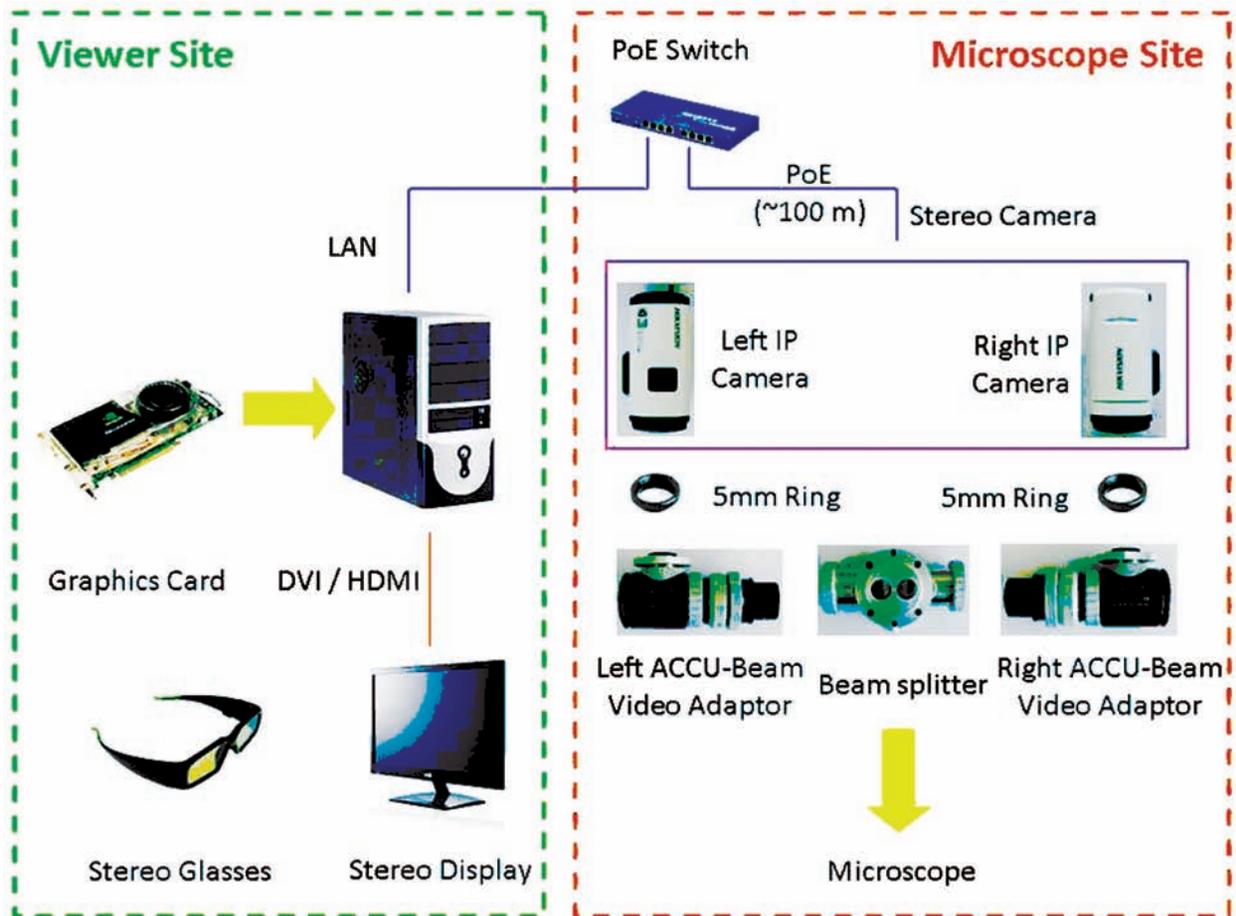
Fig. 1: Architecture of the Trimiti system for neurosurgery training

beam splitter through video adapters [Fig. 1].

Microscope video adaptors facilitate connecting imaging sources to microscope beam splitter and controlling the field of view of the image/video capture. Universal parafocal zoom video adaptor is employed to provide multiple magnification levels with appropriate image focusing. Two video adaptors are connected to two ports of the beam splitter. Each video adaptor is a C-mount and compatible with 1/3" size image sensor camera.

A network IP camera pair with 1/3" sensor size with high definition (1280x720p) resolution is employed for stereo image acquisition.

B. Workstation

The workstation having Intel Core i3 3.3Ghz CPU, 4GB RAM, 500GB hard disk and NVIDIA Quadro 600 professional grade graphics card with Windows 7 OS

is used for running our in-house developed software. The software implements capture & record, process workflow and presents the stereoscopic content from the microscope on the 3D display device.

C. 3D display devices

To simulate the depth perception using the stereovision requires delivering a unique, dedicated image to each eye that represents two different perspectives through the 3D display devices. The 3D display devices are based on two technologies: active stereo, which uses alternate frame sequencing with shutter glasses to block light to one eye while the other is showing its appropriate image, and passive stereo, which uses different light polarization to present the left and right view to a viewer who wears passive polarized glasses. We have used NVIDIA 3D Vision Pro technology consisting of 120Hz 3D monitor and eye wear to realize active stereo and passive 3D-TV

to implement passive stereo technology. Active stereo provides better depth perception with full native image resolution [2], where as passive stereo is more comfortable for eyes.

Software Implementation

In this section, we provide software implementation details of the Trimiti system. Real-time stereo image acquisition from IP camera pair is achieved using GStreamer multimedia framework. H-264 compressed image stream with the real time streaming protocol (RTSP) is utilized for real-time performance and network bandwidth saving. The acquired stereo images are then texture mapped, transformed and converted to compatible stereo format of the 3D display devices using the OpenGL library. The graphical user interface has been developed using Qt framework.

The stereo acquisition unit described in the earlier section has two separate cameras and two separate adapters. Even though they are physically aligned, it is difficult to ensure that the left and right image streams are perfectly matched, leading to vertical, zoom and rotation and temporal disparity error.

To present the comfortable stereo view having only horizontal disparity, we have implemented the system calibration process in software to take care of the above mentioned disparity errors by calculating the appropriate image transformations for the left and right image streams. The transformations are then applied to each and every image frame acquired. The accurate calibration and transforming the high resolution images in real time is absolutely critical for providing the acceptable stereo output.

A. System calibration

Traditional camera and stereo calibration processes [2] compute camera, lens and stereo parameters using number of input images of calibration patterns. As microscope is operated at multiple zoom levels, traditional calibration methods cannot be used as viewable volume of microscope is extremely small.

A chessboard pattern with alternating 5mm size 70 squares is utilized for calibration. It is kept under the microscope and 54 internal corners of the pattern are detected. A single input image is utilized to compute calibration parameters. Initially detected corners are arranged in order and then first and last corners forming diagonal are located. These two corners are utilized to compute orientation, scale and horizontal and vertical shift parameters.

B. Real-time stereo image remapping

Each and every pixel within left and right source views needs to be transformed using calibration parameters, which is computationally expensive and it increases with image size [2]. We implemented it by using the functionality provided by OpenGL.

Incoming input images are mapped within GPU memory using OpenGL. Calibration parameters in the form of OpenGL transformations [2] are applied over these stereo images to generate left and right transformed images. Non overlapping regions of these stereo images are removed for better stereoscopic perception. Finally these transformed images are rendered using either OpenGL quad buffering for active stereo or HDMI 1.4(a) frame packing techniques for passive stereo output.

Results

In this section, we discuss competency of our system. The system supports the workflow consisting of capturing, post processing and presenting the live stereoscopic view from the microscope on multiple 3D display devices. It also supports the recording and playback of the sessions. The simultaneous display of active and passive stereo output is also possible [Fig. 2]. The system also has features to fine tune the disparity adjustments, adjusting the field of view and orientation on the 3D display devices for comfortable stereo.

A. Real-time stereo image remapping

OpenCV library utilizes instruction set extensions such as SSE, SSE-2, and AVX for CPU optimization. OpenCV

Fig. 2: The Trimiti system running active and passive stereoscopic vision using surgical microscope

based stereo image remapping is used to benchmark our OpenGL based stereo image remapping module. Our OpenGL module performs approximately 4 times better than OpenCV module [2].

B. System latency

IP cameras introduce system latency [3] due to image encoding-decoding, network delays and rendering delays. The measured network latency of synchronized left and right IP camera pair is 200ms [2], which is just within acceptable limits of an average human reaction time.

Conclusions

In this article, we have discussed design and development of the real-time stereoscopic vision system for neurosurgery training. It is cost effective and comparable to the commercial systems available for general purpose stereoscopic microscopy. The support of active as well as passive stereo output and ability to stream stereo output over the network and in-hose software makes it highly flexible and extensible.

Acknowledgement

We are obliged to Dr. Sekhar Basu, Director BARC, Shri C. K. Pithawa, Ex-Director, E&I Group and Shri R. S. Mundada, Head of Computer Division for offering us this magnificent opportunity to work on this immerging topic. We are also grateful to Dr. Ashish Suri, Department of Neurosurgery, AIIMS, New Delhi whose timely help has proved quite valuable.

References

1. Shete P. P. and et al, "Trimiti - A Real-time Stereoscopic Vision System for Neurosurgery Training using Surgical Microscope", in Proc. of IEEE international conference ICACCI-2015, August 2015. (in press)

2. Shete P. P. and et al, "A real-time stereoscopic viewer for telerobotics using open source software", in Proc. of IEEE international conference ICACCI-2013, August 2013.

3. Jack Jansen, "VideoLat - an Extensible Tool for Multimedia Delay Measurements", in Proc. of ACM international conference MM-2014, November 2014.

Experimental and Modeling Studies for Online Measurement of Amplitude in a Pulsed Column

G. Sugilal, Shashi Kumar, R. Datta and K. Banerjee
Nuclear Recycle Group
and
S. B. Roy, P. Daniel Babu and M. N. Jayaram
Nuclear Recycle Board

Abstract :

An experimental investigation was carried out initially to study the hydrodynamics of pulsed extraction column with nozzle plates. The experiments were conducted in a 50 mm diameter glass column with 26 standard nozzle plates having 23% free area. 30% TBP in Dodecane was used as continuous phase and 3 M Nitric acid as dispersed phase with organic to aqueous flow rates in the ratio of 3:1. Flooding curve was generated by varying pulsation conditions and throughputs. The experimental facility was then used to develop and validate a model-based online amplitude measurement methodology.

Introduction

Pulsed columns are extensively used in spent nuclear fuel reprocessing plants to separate, decontaminate and purify uranium and plutonium [1, 2]. The pulsed column used for solvent extraction is a vertical column with one contact zone containing a number of perforated horizontal plates, two enlarged ends for phase disengagement, one pulse leg for pulsing, and provisions for feeding and withdrawing aqueous and organic streams (see Fig. 1). The plate perforations are usually so small that substantial flows of aqueous and organic phases due to density difference do not occur. However, application of a periodic pulsation can provide additional energy required to force the liquids through the perforated plates and also to break up the liquids into small droplets and thereby, promoting high interfacial area and increased mass transfer.

In the pulse column design, the height of the contacting section is determined by the efficiency of mass transfer and the diameter of the column is determined by the flooding characteristics. Height of the pulse columns used in a nuclear reprocessing plant should be as small as possible in order to reduce the cost of the hot cell. Equipment design variables and operating variables together determine the efficiency and throughput of the pulsed column. The maximum throughput of the pulsed column is governed by flooding, which may be caused by either insufficient or excessive pulsing. Flooding is defined as the condition at which the two phases cannot pass counter-currently through the column resulting in at least one of the phases leaving from the same end of the column that it entered. This usually results in the rejection of the dispersed phase and the formation of a second interface at the opposite end from the dispersed phase outlet. The flow through the column is achieved from the energy provided by the pulsation. This energy input can be expressed as the product of the pulse amplitude (a) and the pulse frequency (f). This product (a f) is used to correlate the extent of flooding in the column [3]. The minimum HTU (height of a transfer unit) values generally occur in an area between 75 and 95% of the flooding conditions [4]. Therefore, the flooding curve contains basic information for selecting the most favourable operating conditions for a given pulsed column.
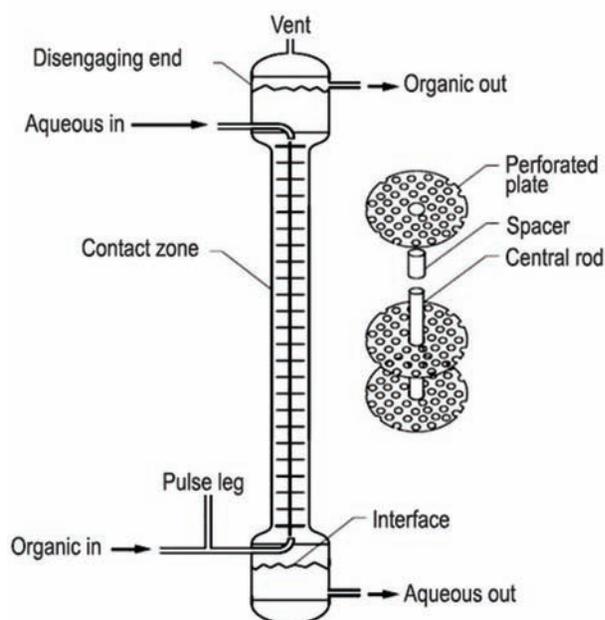
Fig. 1: Schematic of a pulsed solvent extraction column [2]

Experimental setup

In the present study, an experimental investigation was carried out initially to study the hydrodynamics of pulsed extraction column with nozzle plates. The experimental facility was used subsequently to develop and validate a model-based online amplitude measurement methodology.

The experimental setup is shown in Fig. 2. A pilot scale, glass pulsed extraction column with nozzle plates was used for all the experiments undertaken. The vertical glass pulsed column has a 1.5 m long contact zone with an inside diameter of 50 mm. The contact zone is formed by 26 stainless steel nozzle plates oriented downward and spaced 50 mm apart. Each plate is 1 mm thick and contains holes of 4.8/3.2 mm diameter and 1 mm indentation. The holes were laid out on a triangular pitch of 9.5 mm. The free area
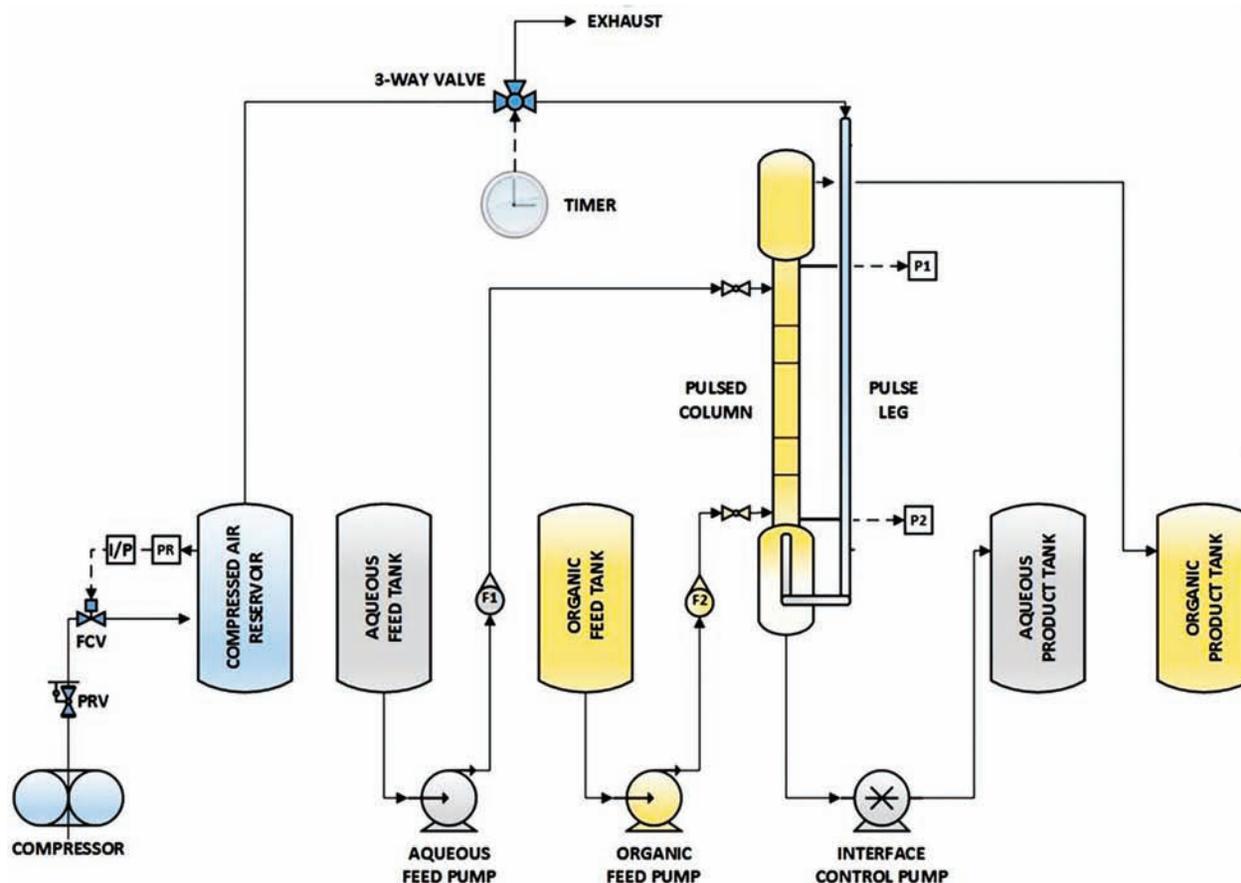
Fig. 2: Schematic of the experimental set up

was approximately 23% of the total area. The phase disengaging ends of the glass column are 600 mm long and have an inside diameter of 150 mm.

The air pulsing system comprises of an air compressor, a pressure regulating valve (PRV), a flow control valve (FCV), an air reservoir with a capacity of 500 L, a 3-way poppet type pulsing valve with electronic timer, a pulse leg and associated piping. The pulse leg is 2.5 m long and has an inside diameter of 25 mm. The PRV is provided to set the line pressure in the upstream side of the FCV, which regulates the compressed air flow to the reservoir and thereby maintains the tank pressure at a set value. The pulse column is provided with two pressure transducers, P1 and P2, to measure the differential pressure across the contact zone (see Fig. 2).

As shown in Fig. 2, the experimental facility is equipped with four stainless steel tanks (1000 L capacity each) for storing the feed and product streams and has provisions for pumping the organic (30% TBP in Dodecane) and aqueous (3M Nitric acid) feed streams to the pulsed column, and measuring their flow rates (F1 and F2). The organic product stream overflows from the column top disengaging end to the organic product tank. The aqueous product stream is withdrawn from the bottom disengaging end using a metering pump which maintains the bottom interface at the desired level.

Experimental procedure

The pulsed column was initially filled with 3M Nitric acid using the aqueous feed pump. Air pulsing was started under static column condition (without liquid feeds) to evaluate the performance of the air pulsing system. An initial static pulsing test was conducted without flow control valve to assess the effectiveness of pressure regulating valve (PRV) in regulating the air pressure in the reservoir. Test results indicated substantial fluctuations in the reservoir pressure which in turn resulted in unsteady pulsing of the liquid column. A flow control valve (FCV) with pressure feedback was introduced to regulate the compressed air flow and thereby, maintain the air

reservoir pressure at the set value. Reservoir pressure transients with and without flow control valve are compared in Fig. 3, which illustrates that introduction of a flow control valve leads to better control on the air reservoir pressure and thus, stable pulsing of the column.
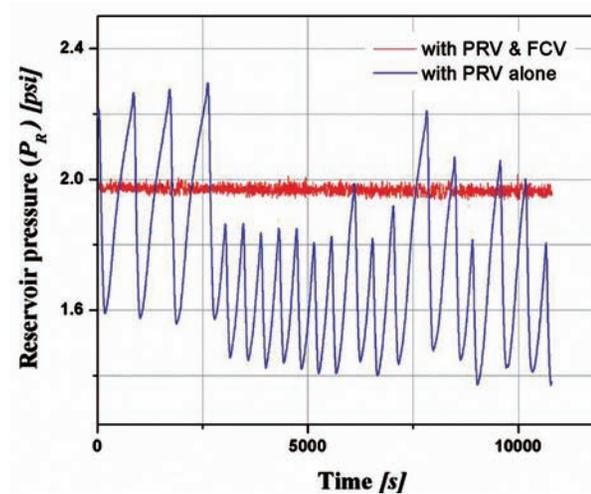
Fig. 3: Compressed air reservoir pressure transients with and without flow control valve

Dynamic pulsing experiments were carried out subsequently using 30% TBP in Dodecane as continuous phase and 3 M Nitric acid as dispersed phase with organic to aqueous flow rates in the ratio of 3:1. The pulsing frequency was maintained at 1 Hz in all experiments. The pulse amplitude was measured by observing the maximum displacement of liquid in the pulse leg with the help of a scale fixed on it. The corresponding amplitude in the actual column was calculated based on the difference in cross sectional areas of the leg and the column. The superficial velocities of organic (VC) and aqueous (VD) in the column were calculated based on the measured volumetric flow rates.

Flooding curve and flow regimes

Flooding curve for the glass pulsed column with nozzle plates was generated by varying the pulse amplitude for a given set of superficial velocities of the liquid feed streams. An O/A ratio of 3 was used in the present study. The pulse frequency was set at 1 Hz using an electronic timer and the pulse amplitude was regulated by adjusting the reservoir air pressure.

Flooding points corresponding to insufficient pulsing and excessive pulsing were obtained for different values of volumetric velocity (VC+VD). These points are presented as flooding curve in Fig. 4. When the volume velocity is 5 mm/s, flooding due to insufficient pulsing occurs at a pulse velocity, a f = 2.5 mm/s and flooding due to excessive pulsing occurs at a f = 55 mm/s. Point 1 in Fig. 4 corresponds to VC+VD = 5 mm/s and a f = 15 mm/s. Fig. 5(1) presents the flow regime corresponding to Point 1 which shows that mixer-settler zone exists under this condition. It was observed that emulsion zone prevails when a f ≥ 25 mm/s. For example, Fig. 5(2) shows the emulsion flow regime corresponding to Point 2, for which VC+VD = 5 mm/s and a f = 30 mm/s
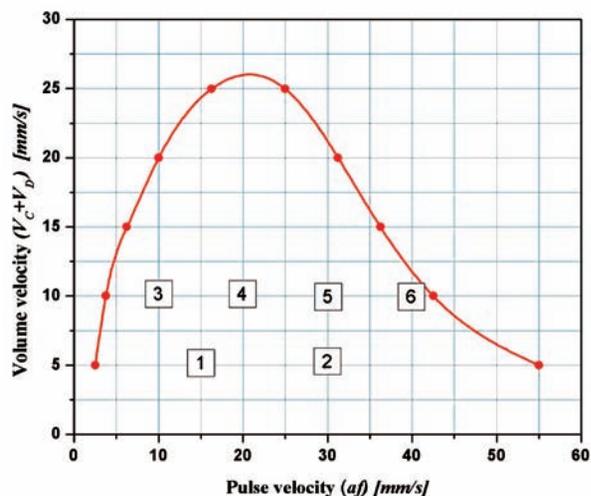
Fig. 4: Flooding curve for pulsed column with nozzle plate (O/A = 3, f = 1 Hz)

(see Fig. 4). Figs. 5(1) and 5(2) illustrate substantial enhancement in the interfacial mass transfer area at Point 2 compared to Point 1. Points 1 and 2 correspond to 27 % and 60 %, respectively, of the flooding a f for VC+VD = 5 mm/s under excessive pulsing condition.

Fig. 6 presents effect of pulse amplitude when the volume velocity is VC+VD = 10 mm/s while maintaining the pulse frequency at f = 1 Hz and O/A=3. Panels (1), (2), (3) and (4) shown in Fig. 6 correspond, respectively, to Points 3, 4, 5 and 6 in Fig. 4. Flow visualization studies conducted confirm that mixer-settler flow regime exists when a f < 25 mm/s and emulsion zone prevails when a f ≥ 25 mm/s. The experimental results establish that for a pulsation frequency, f = 1 Hz, emulsion flow regime occurs when the pulse amplitude, a ≥ 25 mm. Thus, the present study ascertains the importance of on-line measurement of pulse amplitude to operate the pulse column in the most efficient flow regime (emulsion zone).

On-line amplitude measurement in glass column

The present experimental facility was used further to obtain a relation between the differential pressure across the contact zone and pulse amplitude in the column. Pulsing experiments were carried out using single phase flow under dynamic conditions for this
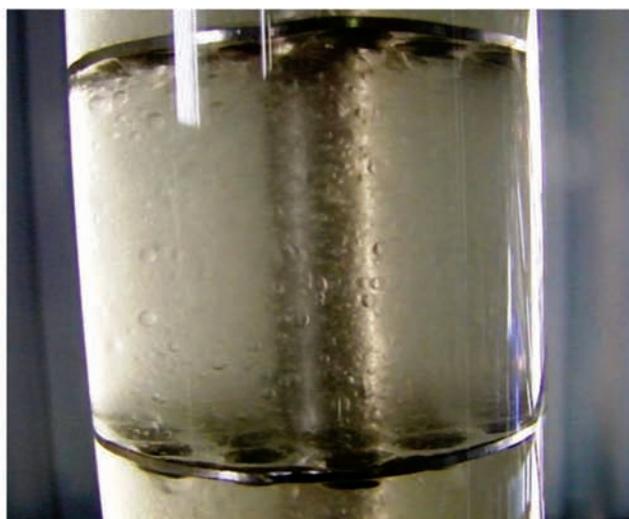
(1) Mixer-settler zone (a =15 mm, f = 1 Hz)

(2) Emulsion zone (a =30 mm, f = 1 Hz)

Fig. 5: Different flow regimes for volume velocity 5 mm/s (O/A = 3)

purpose. Two pressure transducers (Make: CEMEAS, Model: U5156) were used to measure the differential pressure across the contact zone of the column and the data was recorded by a multi channel chartless recorder (Make: EUROTHERM, Model: 6100A). Fig. 7 shows the experimentally obtained differential pressure for pulsing amplitude of 1 inch in the 2 inch diameter glass column. It is observed from Fig. 7 that a low frequency component is superimposed over the high pulsing frequency. Therefore, a time-averaged differential pressure was obtained across the pulsed column based on the area under the differential pressure curve for the period corresponding to the low frequency component.

In order to establish the relation between the time-averaged differential pressure and the pulse amplitude in the column, different experiments were conducted by varying the pulse amplitude from 0.5 inch to 1.5 inch in the 2 inch diameter glass pulse column. The experimental results are presented in Fig. 8. It shows that the pulse amplitude in the 2 inch diameter glass column exceeds 1 inch when the time-averaged differential pressure across the contact zone is more than 2000 Pa. Thus, the time-averaged differential pressure can be used for the near-online calculation of the amplitude in the pulse column based on the amplitude-differential pressure relationship (see Fig. 8).

(1) Mixer-settler zone (a =10 mm)

(2) Mixer-settler zone (a =20 mm)

(3) Emulsion zone (a =30 mm)

(4) Emulsion zone (a = 40 mm)
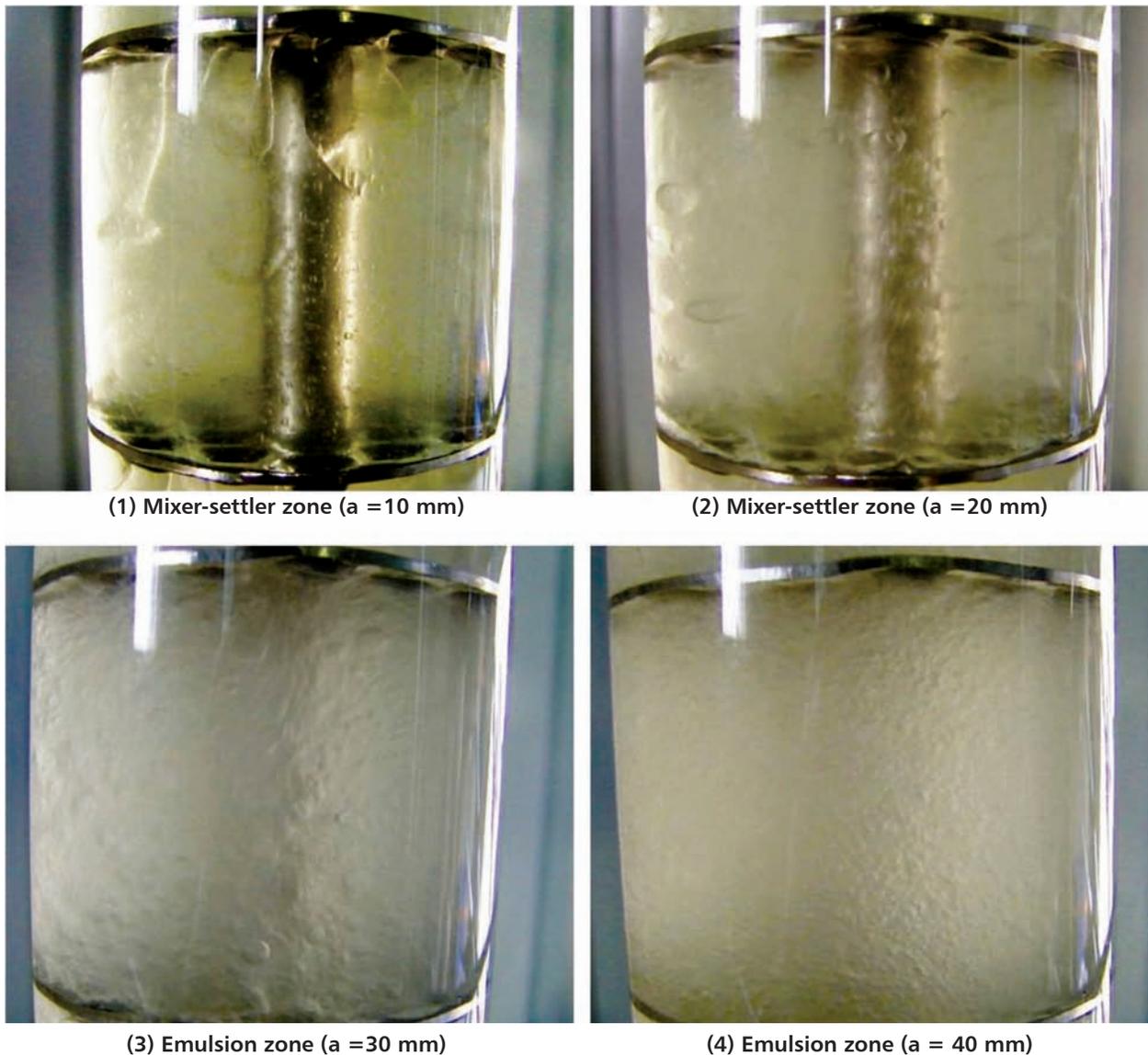
Fig. 6: Effect of amplitude for volume velocity of 10 mm/s (f = 1 Hz, O/A=3:1)

As it is difficult to generate the amplitude-differential pressure relationship for an industrial pulsed column experimentally, a model-based methodology was developed for the on-line measurement of pulse amplitude in the reprocessing plants. A mathematical model for the air pulsing can be used to generate the relation between the amplitude and differential pressure in the pulsed column. Such a model comprises of three sets of governing equations – first set of equations for describing the air behaviour during air supply to the pulse leg, second set for describing the air behaviour during air exhaust from the pulse leg and third set for describing the liquid behaviour

in the pulse leg and the column. Formulation and solution of these governing equations are described in [5, 6, 7] and not described here. Fig. 9 compares the model predicted amplitude-differential pressure relationship with that obtained experimentally. It shows that the model predictions agree well with the experiments and the maximum error is about 10% when compared with the experiments using a 2 inch diameter glass column. Fig. 9 also shows a uniform under-prediction of the experimental results by the model. This is on account of the fact that the pressure transducers used in the experiments could record only 8 measurements per cycle, thereby,
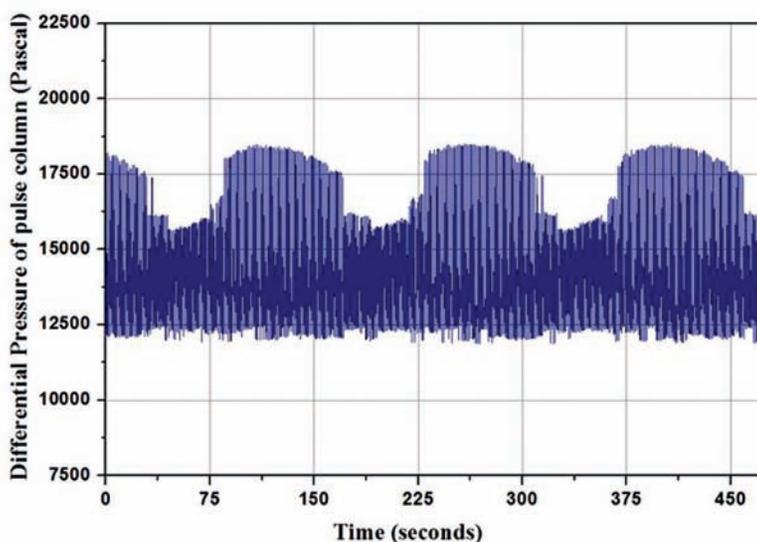
Fig. 7: Differential pressure across the 2 inch glass column for 1 inch amplitude
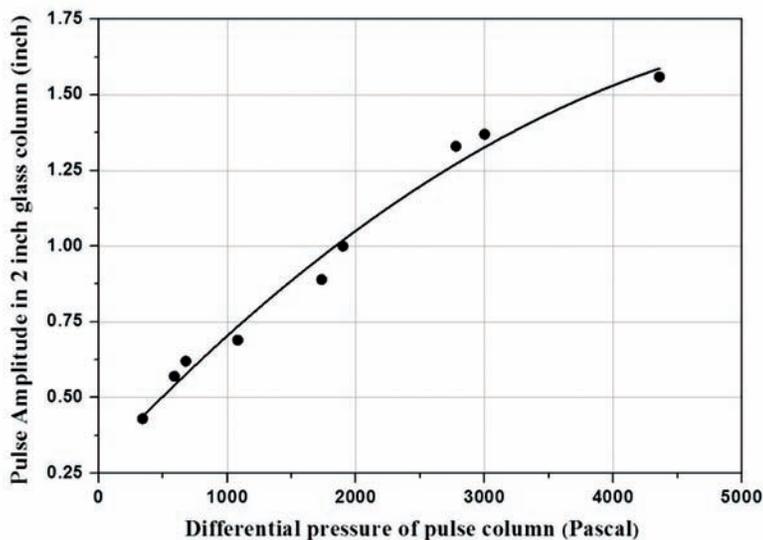
Fig. 8: Pulse amplitude as a function of time-averaged differential pressure

resulted in a uniform under-prediction in the area-averaged differential pressure. Since purge method will be used for pressure measurement in the actual plant, the temporal variation in the differential pressure can be smooth and less noisy compared to that obtained using a pressure transducer. This will reduce the error between the measured values and the model predictions. In case of industrial columns, the mathematical model needs to be tuned based on the static pulsing experiments during commissioning. The tuned model can be used to generate a calibration curve for calculating the pulse amplitude in the column based on online measurement of the differential pressure across the contact zone.

Conclusions

The present study establishes the importance of on-line measurement of pulse amplitude to operate the pulse column in the most efficient flow regime. The experimental results shows that a pulse amplitude of $a \geq 25$ mm is required to maintain emulsion flow regime for a pulsation frequency of $f = 1$ Hz. From the experimental data, it is ascertained that the time-averaged differential pressure can be used for the near-on-line calculation of the amplitude in the pulse column based on the amplitude-differential pressure relationship. This study also illustrates that a mathematical model for the air pulsing can be used to generate the relation between the amplitude and differential pressure in the column. The mathematical model can be tuned based on the static pulsing experiments during commissioning. The tuned model can be used to generate a calibration curve for calculating the pulse amplitude in the column based on online measurement of the differential pressure in the plant.

References

1. M. Benedict, T. H. Pigford, H. W. Levi, Nuclear Chemical Engineering, McGraw-Hill, 1981.

2. M. F. Simpson, J. D. Law, Nuclear fuel reprocessing, Idaho National Laboratory, INL/EXT-10-17753, 2010.

3. G. H. Beyer, R. B. Edwards, Flooding characteristics of a pulse extraction column, Ames Laboratory, ISC-553, 1954.

4. G. A. Nicholson, Purex pulse column studies with hydrocarbon diluent, Volume 1, General Electric Co., Richland, WA, HW-40550, 1956.

5. M. E. Weech, B. E. Knight, Design of air pulsers for pulse column application, I&EC Process Design and Development, Vol. 6, No. 4, 1967.

6. G. Sugilal, K. N. S. Nair, Characteristics of air pulsing used in pulsed solvent extraction columns, BARC Report, BARC/20012/I/005, 2012.

7. S. B. Roy, Online amplitude measurement in pulsed columns, M. Tech Thesis, Homi Bhabha National Institute of Technology, 2015.

Development of Methodology for Separation and Recovery of Uranium from Nuclear Wastewater

S.K. Satpati and S.B. Roy
Uranium Extraction Division
and
Sangita Pal and P.K. Tewari
Desalination Division

Abstract :

Uranium plays a key role in nuclear power supply, demand of which is growing up with time because of its prospective features. Persistent increase in different nuclear activities leads to increase generation of nuclear wastewater containing uranium. Separation and recovery of the uranium from its unconventional source like nuclear wastewater is worth to explore for addressing the reutilisation of the uranium source. It is also necessary to improve remediation technology of nuclear industries for environmental protection. Development of a suitable process methodology is essential for the purpose to supersede the conventional methodology. In the article, recent developments in several possible methodologies for separation of uranium from dilute solution have been discussed with their merits and demerits. Sorption technique as solid phase extraction methodology has been chosen with suitable polymer matrix and functional moiety based on wastewater characteristics. Poly-hydroxamic Acid, PHOA sorbent synthesized following eco-friendly procedure is a promising polymeric chelating sorbents for remediation of nuclear wastewaters and recovery of uranium. Sorption and elution characteristics of the PHOA have been evaluated and illustrated for separation and recovery of uranium from a sample nuclear wastewater. For the remediation of nuclear wastewater SPE technique applying the PHOA, a polymeric sorbent is found to be a potentially suitable methodology.

Introduction

Unhindered growth of a nation depends on energy security which is the availability of natural resources for energy consumption. There is an acute demand for more and more reliable power supplies. Nuclear power will be playing a key role in near future for reliable power supply of India and about 25% nuclear contribution in the power supply is the ambition for year 2050 [1]. Uranium has been projected as the main workhorse of future fuel and it gives large amount of power using a small amount of fuel and space. Due to limited reserve of natural uranium in India it is required to explore various other resources of uranium including secondary resources and unconventional sources to meet the long term energy sustainability of Indian nuclear programme [2]. It is important and necessary to recognize the concern over the environmental and health impacts in parallel

to ensure a long term supply of uranium to sustain any country's nuclear power program. As a result of the developments that have taken place world wise in the areas of uranium recovery from unconventional sources or from its lean solution, the philosophy and the concept of the processing of the plant effluent have changed from the traditional methodology. Thus, the uranium recovery technique or separation methodology should be recognized as having a bright future.

The amount of uranium in the environment has exceeded due to activities of nuclear industry, mineral extraction, uranium combustion, mining processes and use of phosphate fertilizer that contains uranium. As per the World Health Organization (WHO) standards, the maximum acceptable concentration of U(VI) in water is 50 mg L-1 [3]. Toxicity of uranium is closely associated with its solubility. In regions of radioactive

contamination of local soil and groundwater, the chemical toxicity of uranium has aggravated health concerns. Water and soil contamination with uranium ions has become a global environmental problem. Even at low concentrations, because of their persistent and accumulative nature these are toxic. Therefore, separation and recovery of uranium are of great practical significance.

Uranium separation techniques

Toxic metals like uranium can be removed from wastewaters, for the clean-up process, by a number of separation technologies, such as chemical precipitation, membrane process, solvent extraction, floatation, coagulation and sorption process. Despite different techniques applied for the remediation of uranium removal from wastewater, it is important to mention that the selection of the most apposite treatment techniques depends on the composition of the wastewater, initial metal concentration, principal investment and operational cost, plant tractability and reliability and environmental impact. Chemical precipitation is applicable for relatively concentrated solution. Floatation process requires addition of uranium specific surfactant or flocculent which is rarely available. Chemical precipitation, coagulation and floatation processes add contamination (organic / inorganic) to the wastewater and recovery of the uranium is difficult. Solvent extraction is recognized as a versatile for laboratory as well as for large scale separation of uranium from different streams. However, separation and recovery of uranium by conventional solvent extraction has some short coming with respect to third phase formation, crude oil formation as well as solvent loss. Moreover, this method cannot be used for effective separation and recovery of metal ions from dilute solutions of alkaline medium. Thus, the development of more efficient techniques has lead to development of liquid-membrane based separation which holds promise for recovery of uranium ions from dilute resources and has received a considerable attention in separation science and technology. Liquid membrane processes are finding increasing application in chemical

industry for achieving energy efficient (with respect to conventional membrane process) and selective separations from very dilute medium. In general two types of liquid membranes - bulk / supported liquid membrane (BLM / SLM) and emulsion liquid membrane (ELM) have been reported widely are being extensively studied, for their application in extraction and concentration of dissolved metals from effluents using various extractants. The problem of low flux rate due to high diffusion resistances, inefficient operation and exorbitant costs encountered in bulk and supported liquid membranes (BLM/SLM) are overcome in an ELM. In the ELM process, an emulsion of organic membrane phase and aqueous inner phase is dispersed in the continuous aqueous feed phase. This gives a highly selective and ultra thin liquid film generating a large mass transfer area for separation. ELM technique has been tried by various workers for recovery of uranium, plutonium and lanthanides from dilute solutions using various carriers. But main disadvantages are the leakage and swelling problems and difficulties in de-emulsification step for which the technology yet to be brought up to industrial scale with full confidence. Hence, solid phase extraction for separation and removal of uranium ions is the method of choice due to its high separation efficiency, good reproducibility of retention parameters, and simplicity and is a popular method owing to its applicability to both pre-concentration and separation [4].

Solid Phase Extraction (SPE)

SPE has additional advantages over other separation techniques such as (i) reduced solvent usage (ii) low disposal costs, (iii) short extraction times, (iv) high efficiency, (v) ecologically-safe, (vi) elimination of some of the glassware, (vii) reduced exposure of analysts to organic solvents (viii) more reproducible results (ix) remote operation etc. In recent years, SPE is the most often used method in trace metal analysis in environment for the separation and/or pre-concentration purposes. Sorption process, a SPE technique, is defined as a surface phenomenon; sorption is the adhesion of a molecule onto the sorbent surface. The sorption proceeds by complex

process affected by several mechanisms involving adsorption by physical forces on surface and pores, chemisorptions, ion exchange, complexation, chelation, and entrapment in capillaries. Due to high affinity of the sorbent for the uranium(VI) ion species, the latter is attracted and bound by the sorbent via these mechanisms.

A solid phase extractant, adsorbent /sorbent consists of two parts: a matrix and functional components. An inert host structure which allows diffusion of hydrated ions i.e. a hydrophilic matrix is an essential part of any sorbent. The selection of the matrix depends on several important criteria of application like regular and reproducible form of its structure, stability in conditions of application medium, option on the type of exchanger etc. The functional group represents the ligand required for metal complexation. The most common coordinating atoms present in the main or side chain are N, O, P and S. It is possible to make chelating sorbent that have a selective adsorption capacity for specific metal ions by fixing the desired ligand groups on the sorbent matrix. Commonly used materials for the matrix can be broadly divided into four groups: (i) Minerals and Inorganic oxides: clay, diatomite, zeolite, alumina, silica, ceramic, tin oxide, iron oxide etc. (ii) Carbonaceous materials: activated carbon (AC), mesoporous carbon, carbon nano-tubes (CNTs), graphite and its derivatives/ grapheme etc. (iii) Biosorbent: Chitosan, yeast, alga, agro-waste etc. and (iv) Polymers/copolymers: resins, hybrid materials/ composites, gels and related materials. For each type of matrix have advantages and disadvantages based on its application. Based on nuclear wastewater characterisation, case specific suitable SPE matrix material is chosen for uranium separation and recovery from nuclear wastewater.

Promising chelating sorbent for uranium extraction

Chelating agents are compounds containing donor atoms (ligands) that can combine by coordinate bonding with metal ion to form an organised structure called as a chelate. Co-ordination between metal – ligand is a Lewis acid – Lewis base neutralization process. Complexing sorbents of new types are developed deliberately; possessing a tailor made structure that would bind the element with the ligand. Ability of a ligand to complex with a target metal ion is also a function of the solution pH and the presence of competing anions. The removal of desirable metal ions from wastewaters and process effluent stream has led to the development of several

Table 1: Major sorbents reported for the uranium separation from dilute solutions

Chemical form	Suitability
Hydrous titanium oxide (developed before 90's)	Difficulty in large scale in submerged mode for seawater application. Low kinetics and capacity.
Macrocylic hexacarboxylic acid (developed before 90's)	Difficulty in production of polymer-bound hexacarboxylic acid.
Amidoxime (developed before 1995) Amidoxime + Methacrylic acid [5]	Most extensively studied, suitable for large scale production in the form of fibres, resin, or grafted fibrous sheet, slow kinetics and limited selectivity. Have advantages of Amidoxime group and show better uranium sorption kinetics. Hazardous synthesis process.
Calixarene-based uranophiles and others	Highly selective towards uranium, slow sorption kinetics, difficulty in anchoring in polymer matrix, synthetic chemistry involved is not suitable for large scale production. Very costly.
2,2'-dihydroxy azobenzene and related chemical groups [6]	Involve synthetic chemistry, not evaluated for real application.
Poly(Hydroxamic Acid) Resin (developed before 90's and recently [7]	Have all advantages of hydroxamic acid group for recovery heavy metals including uranium along with iron. Cheaper, safe synthesis process & easy to dispose.

types of chelating sorbents. Few reportedly important inorganic and potential sorbents for uranium recovery from dilute solutions are mentioned in Table – 1. The diffusion mobility of U(VI), either in $[UO_2(CO_3)_3]^{4-}$ form or UO_2^{2+} form, in the sorbent would be dependent on the physical as well as chemical interactions (electrostatic and covalent) with the ligand-sites in sorbent matrix. As de-complexation of $[UO_2(CO_3)_3]^{4-}$ can be catalyzed by H^+-ions, the presence of acidic monomer or co-monomer with appropriate pKa value may enhance the sorption kinetics of U(VI) in the sorbent from the wastewaters. Considering these parameters, a new sorbent Poly – hydroxamic Acid, PHOA has been evaluated for uranium recovery from a nuclear wastewater.

Evaluation study:

Materials/chemicals such as acrylamide, N, N' methylene bis acrylamide, hydroxyl amine hydrochloride, methanol, acetone, sodium hydroxide, HCl were procured from local market and were used in the synthesis process without further purification. Synthesis route of the sorbent has been chosen carefully to follow safe and economic process. The sorbent has been synthesised by a two-step method: (a) by addition polymerisation of homogeneously mixed acrylamide with a cross-linking agent and in situ gelling of the whole mass followed by precipitation and (b) the crumbled, washed and dried gel was converted into a macro-porous chelating agent by treatment with hydroxylamine hydrochloride. Photograph of the sorbent preparation scheme has been shown in Fig.1.

Sorbent's surface pores are opened up in the water (swelling) because of hydrophilic nature of the sorbent, as designed for the purpose. Suitability tests with synthetic solution indicated that the sorbent can be used for sorption process in alkaline medium and for elution process in HCl medium. Equilibrium capacity was found to be 1.1 mg/g of sorbent with distribution coefficient 2500 mL/g of sorbent. Treated raffinate filtrate of uranium processing plant, wastewater was characterized and composition analysis shows that it contents uranium 5 – 10 mg/L and Mg, Ca and nitrate ions (all g/L level) along with low concentration of Fe, Cu, Mn (<5 mg/L) and the wastewater is alkaline in nature (pH>7). An Inductively Coupled Plasma Emission Spectrophotometer (ICPAES), Jobinyvon Emission, Model No. JY 328 was used to determine uranium and other metal ions' concentrations in solutions. Batch experiments were carried out in laboratory scale at room temperature (RT).

Fig. 1: Preparation scheme of PHOA

Virgin PHOA

Uranium loaded PHOA
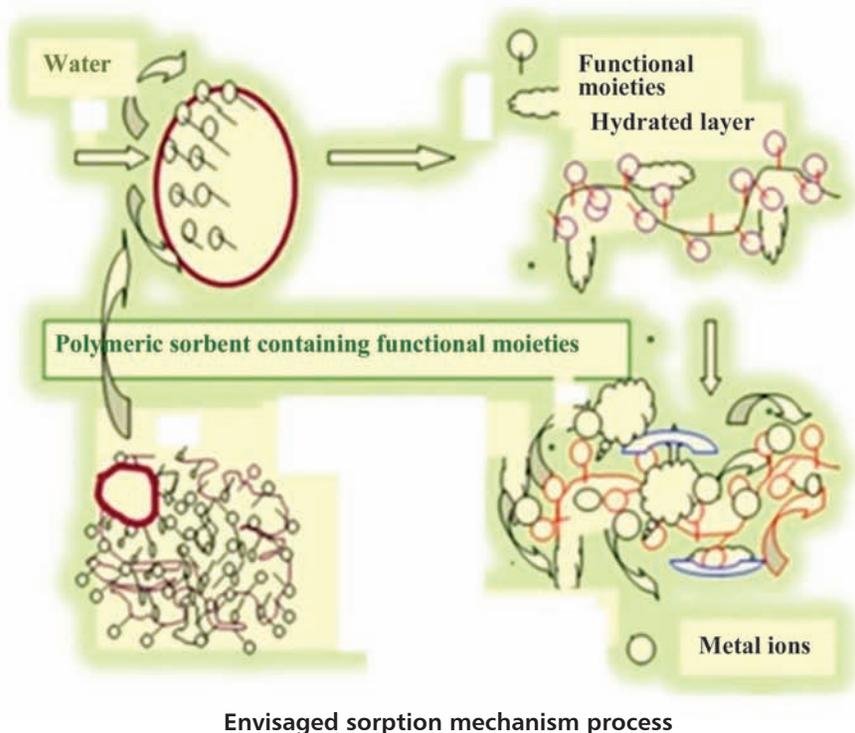
Envisaged sorption mechanism process

Fig. 2: Uranium sorption onto PHOA sorbent

Appearance of virgin PHOA and PHOA loaded with uranium from the wastewater along with envisaged sorption process has been shown in Fig. 2. Uranium sorption onto PHOA has been establish by energy-dispersive X-ray spectroscopy (EDS) analysis as well as Fourier transform infrared spectroscopy (FTIR) analysis of the uranium sorbed PHOA which is depicted in Fig. 3. The sorption reaction between PHOA and U(VI) was investigated for its kinetics and mechanism. As shown in Fig. 4, the process follows the monolayer molecule sorption procedure. It also reflects that chemical sorption may be the pathway

for the chelating reaction between U(VI) and PHOA. The Boyd plot indicates that external mass transfer is not the rate limiting step in the process and the rate is controlled by both, intra-particle diffusion or metal-ligands interaction.

The results of efficiency of different chemical agents as eluents are shown in Fig. 5 which has been articulated in the mechanism of sorption process in Fig. 2. Inorganic acids are found to be more efficient eluent than others. To avoid damages of sorbent structure application of oxidising acids has been
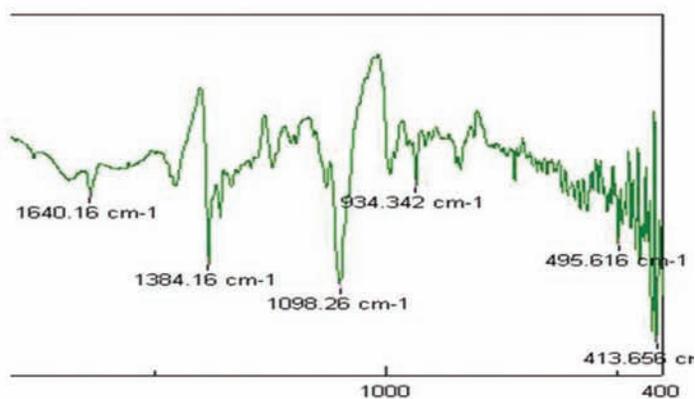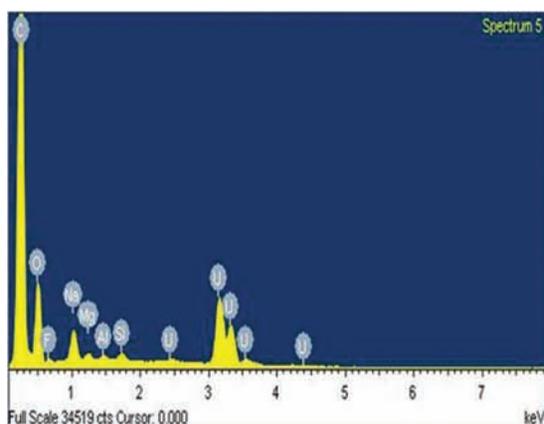
Fig. 3: Instrumental analysis of U(VI) loaded PHOA
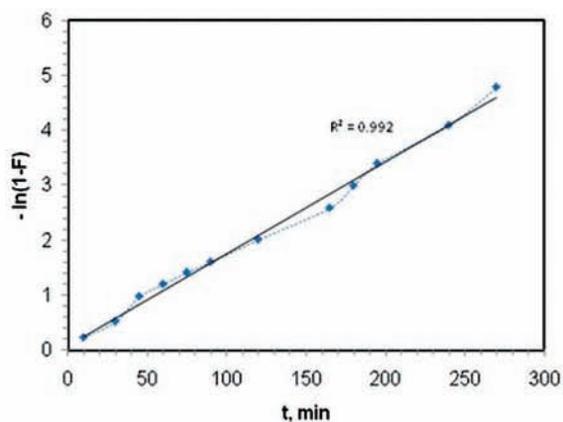
Monolayer sorption of U(VI) onto PHOA:
F = (qt/qe), q is uptake
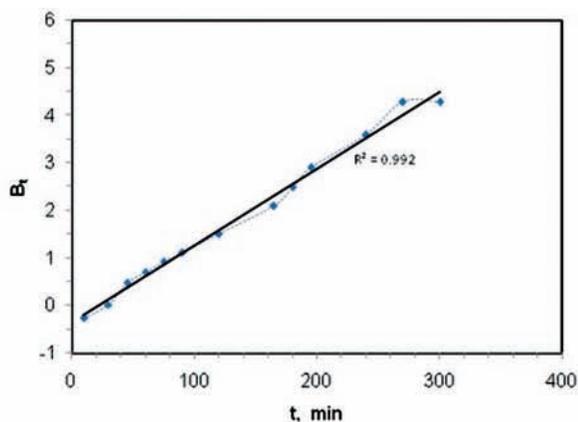
Boyd plot for U(VI) sorption onto PHOA: B_t=
-0.4977-ln-(1-F)

Fig. 4: Kinetics and mechanism of the sorption process
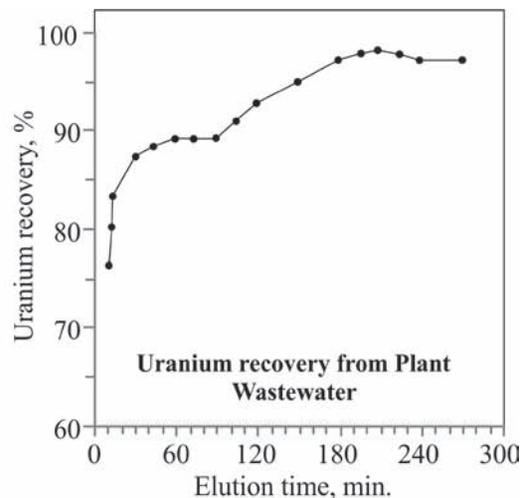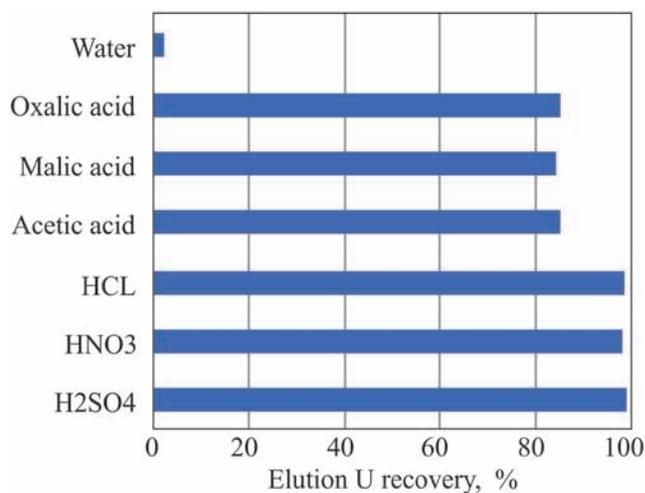
Fig. 5: Elution of uranium from loaded PHOA sorbent

**Fig. 6: Uranium recovery methodology from
nuclear wastewater using PHOA**

avoided. Hence, HCl has been chosen as effective eluent and more than 97% uranium recovery is achieved within 3h time.

Fig. 6 describes the uranium recovery methodology from nuclear wastewater using PHOA as solid phase extractant with six times regeneration capacity. The experimental studies are indicative of the fact that Uranium recovery from wastewater generated in nuclear establishment using novel sorbent, PHOA is viable and technologically implementable.

Conclusion

Uranium although present in low level (<10 mg/L) in nuclear wastewater, can be separated and recovered by the developed SPE methodology, which is better in choices. The process envisages deploying the possibility of harnessing uranium from nuclear wastewater. This also indicates that the methodology is available well in hand to polish the wastewater if required in future. As a matter of case study, a wastewater of uranium processing plant has been adopted for the evaluation of methodology which has been successfully demonstrated for separation and recovery of uranium.

References

1. Integrated Energy Policy: Report of the Expert Committee. Planning Commission Document, Government of India, (2006) 1-147.

2. C.K. Gupta and H. Hingh, "Uranium Resource Processing: Secondary Resources", Springer, Germany, (2003).

3. WHO, Guidelines for Drinking Water Quality, 3rd edition, (2003).

4. M.S. Hosseini, A. Hosseini-Bandegharaei, J. Hazard. Mater. 190 (2011) 755–765.

5. K. Saito, K.Sugita, A.Katakai, N. Seko, T. Sugo, J. Kanno, T. Kawakami, Ind. Engg. Chem. Res. 39 (2000) 2910.

6. B.B. Jang, K. Lee, W.J. Kwon, J. Suh, J. Poly. Sci.: Part A: Poly. Chem. 37 (1999) 3169.

7. S. Pal, S.K. Satpati, K.N. Hareendran, S.A. Kumar, K.L. Thalor, S.B. Roy, P.K. Tewari, Int. J. Nucl. Desalination 4 (1) (2010) 28-36.

BARC Scientists Honoured

Dr Surinder Mohan Sharma, Director, Physics Group has been elected a Fellow of the Indian National Science Academy, New Delhi. Dr Sharma has been a Fellow of the Indian Academy of Sciences, Bangalore and the National Academy of Sciences, Allahabad. Dr S M Sharma, through his sustained work on studying materials under extreme environments, has established some unique phase transitions, particularly high pressure amorphization. He has developed three synchrotron beam lines, namely X-ray diffraction under extreme conditions, protein crystallography and IR absorption in INDUS-II in RRCAT, Indore.

Dr Gautam Kumar Dey, Associate Director, Materials Group and Head, Materials Science Division has been elected a Fellow of the Indian National Science Academy, New Delhi. Dr G K Dey is a recipient of Indian Institute of Metals G D BIRLA GOLD medal for the year 2011. He is a fellow of the Indian National Academy of Engineering. Dr G K Dey's original work on zirconium based amorphous alloys has opened up a host of all metallic amorphous alloys including bulk metallic glasses. His work also encompasses engineering materials such as zirconium and nickel based alloys being extensively used in India's nuclear programme. He is one of the best electron microscopist of the country and has employed a variety of novel TEM techniques to unfold complex microstructures.

Modular Lab at BARC